AIAA JOURNAL
Vol. 30, No. 4, April 1992

Effect of Surface Deformation on Thermocapillary Bubble Migration

J. C. Chen* and Y. T. Lee†
National Central University, Chung-Li, Taiwan 32054, Republic of China

Under microgravity environments, the thermocapillary migration of a deformable gas bubble placed in a liquid with a constant temperature gradient is investigated numerically. A finite difference method with boundary-fitted coordinates is employed to solve the axisymmetric governing equations. An iterative procedure is introduced for the computation of the deformable shape and the thermal velocity of the gas bubble. The influence of the Marangoni and capillary numbers is considered. Results of the computations show that the terminal velocity of the gas bubble is reduced significantly by the effect of surface deformation.

Nomenclature

A = temperature gradient far from the gas bubble
Ca = capillary number
Ma = Marangoni number
Pr = Prandtl number
p = dimensionless pressure
p' = dimensional pressure
R = dimensionless shape function of the bubble surface
R' = shape function of the bubble surface
Re = Reynolds number
r = dimensionless radial coordinate
r_b = radius of undeformed gas bubble
r' = dimensional radial coordinate
T = dimensionless transformed temperature
T_o = reference temperature
T' = dimensional temperature
$\overline{T}$ = dimensional transformed temperature
t = time
u, u' = dimensionless and dimensional radial velocity, respectively
v, v' = dimensionless and dimensional azimuthal velocity, respectively
α = thermal diffusivity
γ = surface-tension temperature coefficient
θ = azimuthal coordinate
μ = dynamic viscosity
ν = kinematic viscosity
ρ = density
σ_0 = mean value of surface tension
ϕ = angular coordinate
ψ = stream function
ω = vorticity

Subscripts

r, θ = derivatives with respect to r, θ
∞ = value far from the gas bubble

Introduction

A GAS bubble placed in a fluid which exhibits a temperature gradient will move toward the hotter portion of the fluid field due to the thermocapillary force. Usually, this effect is overshadowed by the buoyancy force exerted on the gas bubble due to the presence of gravity. Under microgravity environments, however, the thermocapillary migration becomes significant. Recently, the thermocapillary migration of a gas bubble in a surrounding fluid medium has drawn significant attention because this effect can be used to control the location of bubbles during the processing of materials in microgravity environments.

The problem of thermocapillary migration of a gas bubble was first investigated, both theoretically and experimentally, by Young et al.[1] They demonstrated experimentally that the bubble can be driven by means of a thermocapillary force. In the theoretical work, they determined the thermal velocity of a gas bubble by solving the momentum and energy equations without the consideration of the effects of convective transport and inertia. Bratukhin[2] used a perturbation expansion to obtain a terminal velocity valid for small Reynolds number. Subramanian[3] employed a matched asymptotic expansion procedure with the Marangoni number as a parameter. His results show that the terminal velocity is reduced by the presence of the convective transport of energy. Shankar and Subramanian[4] calculated the terminal velocity numerically for small Reynolds number and Marangoni numbers up to 2×10^2. Computations performed by Balasubramaniam and Lavery[5] had been carried out for Reynolds numbers from 10^{-7} to 2×10^3 and Marangoni numbers from 10^{-7} to 10^3. In all of the previous theoretical work, the bubble boundary is assumed spherical. Balasubramaniam and Chai[6] determined the shape of the bubble for a small Marangoni number and an arbitrary Reynolds number when the deformations from the spherical shape are small. But they did not consider the effect of deformation of the bubble surface on the terminal velocity.

Because of the nonuniform distribution of surface tension along the bubble surface, the bubble will be deformed from the spherical shape no matter how small the temperature gradient of the fluid is. The effect of deformation of the bubble surface on the terminal velocity has not been explored yet. The existing literature on numerical simulation of deformable bubble problems is quite limited. This is because of the formidable difficulties that arise when solving the governing equations with deformable free surface. Ryskin and Leal[7] developed a numerical technique based on a finite difference approximation of the equations of motion on an orthogonal curvilinear coordinate system to solve the problem of a deformable gas bubble that undergoes a buoyancy-driven motion through a quiescent fluid. This problem is also studied by Christov and Volkov[8] using a finite difference method with a coordinate transformation. In their approach, the bubble motion induced by buoyancy is replaced by a given rising velocity. An infinite liquid moves with a uniform velocity

Received Oct. 30, 1990; presented as Paper 91-0312 at the AIAA 29th Aerospace Sciences Meeting, Reno, NV, Jan. 7–10, 1991; revision received April 10, 1991; accepted for publication April 12, 1991.

*Professor, Department of Mechanical Engineering.
†Graduate Student, Department of Mechanical Engineering.

toward the stationary bubble. Therefore, the thermal field does not need to be considered in their studies.

In the present study, the influence of surface deformation on the terminal velocity of thermocapillary bubble migration in an infinite medium with a linear temperature distribution is investigated by a series of numerical computations. The numerical scheme for integrating the nonlinear governing equations with boundary conditions is a modified version of that used by Chen et al.[9,10] and Lee and Chen.[11] In contrast to previous studies,[1-6] both the terminal velocity and the shape of the gas bubble are determined as parts of the solution.

Mathematical Formulation

Consider a gas bubble present in an infinite liquid region that exhibits a linear temperature variation of slope A along the z axis. Because of thermocapillary effects, the bubble will move toward regions of higher liquid temperature with a constant terminal velocity V_∞. In the present study, the influence of gravity is neglected and the flow is assumed to be incompressible and Newtonian with constant physical properties, except that the surface tension is a monotonically decreasing function of temperature. The viscosity and the thermal conductivity of the gas are assumed to be small compared to those of the liquid.

Here we use spherical coordinates (r', θ, ϕ) with the origin at the center of mass of the bubble (see Fig. 1). Far away from the bubble, the fluid approaches it at the constant velocity V_∞, and the temperature field is unsteady as viewed from an observer located at the origin. For convenience, the new steady temperature field $\overline{T}$ is defined by

$$\overline{T} = T' - V_\infty A t - T_o \tag{1}$$

The problem is assumed to be symmetric in the ϕ direction, and the gas-liquid interface is described as $r' = R'(\theta)$.

We introduce the following nondimensional variables:

$$r = r'/r_b, \quad u = u'/u^*, \quad v = v'/u^*, \quad v_\infty = V_\infty/u^*$$

$$T = \overline{T}/(Ar_b), \qquad R = R'/r_b, \qquad p = p'/(\gamma A)$$

where $u^* = \gamma A r_b/\mu$ is the characteristic velocity. Eliminating the pressure, the dimensionless equations governing the steady, axisymmetric motion of liquid can be expressed in the following form:

$$Re\left(\frac{-1}{r}\psi_\theta\omega_r + \frac{1}{r}\psi_r\omega_\theta + \frac{1}{r^2}\omega\psi_\theta - \frac{1}{r}\psi_r\omega\cot\theta\right)$$
$$= \left(2\omega_r\sin\theta + r\omega_{rr}\sin\theta - \frac{1}{r\sin\theta}\omega + \frac{1}{r}\omega_\theta\cos\theta + \frac{1}{r}\omega_{\theta\theta}\sin\theta\right) \tag{2a}$$

$$Ma\left(v_\infty - \frac{1}{r^2\sin\theta}\psi_\theta T_r + \frac{1}{r^2\sin\theta}\psi_r T_\theta\right)$$
$$= \left(\frac{2}{r}T_r + T_{rr} + \frac{1}{r^2}T_{\theta\theta} + \frac{1}{r^2}T_\theta\cot\theta\right) \tag{2b}$$

$$r\omega\sin\theta = \psi_{rr} + \frac{1}{r^2}(\psi_{\theta\theta} - \psi_\theta\cot\theta) \tag{2c}$$

Here, the stream function ψ is defined as

$$u = \frac{1}{r^2\sin\theta}\psi_\theta, \qquad v = \frac{-1}{r\sin\theta}\psi_r \tag{3}$$

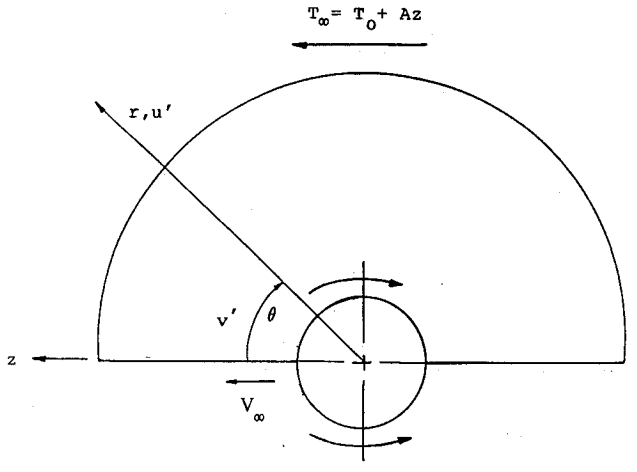

Fig. 1 Schematic diagram of the physical system.

and the vorticity is given by

$$\omega = \frac{1}{r}v + v_r - \frac{1}{r}u_\theta \tag{4}$$

The parameters appearing in Eqs. (2) are

Reynolds number:

$$Re = u^* r_b/\nu = \gamma A r_b^2/(\mu\nu)$$

Marangoni number:

$$Ma = PrRe = \gamma A r_b^2/(\mu\alpha)$$

where the Prandtl number is given by $Pr = \nu/\alpha$.

The boundary conditions at $r \to \infty$ are

$$\psi = -v_\infty r^2\sin\theta^2/2, \qquad \omega = 0$$

$$T = r\cos\theta\,(0 \le \theta \le \pi) \tag{5a}$$

The velocity and temperature fields and bubble shape are symmetric at $\theta = 0$ and π.

$$\psi = 0, \qquad \omega = 0, \qquad T_\theta = 0 \tag{5b}$$

Because a gas bubble would have a very low heat transfer coefficient, the adiabatic condition at the bubble surface is assumed. The jump in the normal stress across the interface is balanced by the surface tension times the mean curvature, whereas the jump in the shear stress equals the surface-tension gradient along the deformable bubble surface. The boundary conditions for the gas-liquid interface $[r = R(\theta)]$ are

$$\psi = 0 \tag{5c}$$

$$-p + 2\left[\frac{-\psi_{\theta r} + \psi_\theta/R - R_\theta\psi_{rr}}{R^2\sin\theta} - \frac{R_\theta}{2R}\omega\right]$$
$$= Ca^{-1}\left[\frac{R^2 + 2R_\theta^2 - RR_{\theta\theta}}{(R^2 + R_\theta^2)^{3/2}} + \frac{|R_\theta\cos\theta - R\sin\theta|}{R\sin\theta(R^2 + R_\theta^2)^{1/2}}\right]$$
$$\times (1 - CaT) \tag{5d}$$

$$\omega = \left[2\left(\frac{-\psi_r}{R^2 \sin\theta} + \frac{\psi_{rr}}{R \sin\theta}\right) + \frac{R^2}{(R^2 - R_\theta^2)(R^2 + R_\theta^2)^{1/2}} \times \left(\frac{R_\theta}{R} T_r + T_\theta\right) + \frac{2R_\theta R}{R^2 - R_\theta^2} \times \left(\frac{3}{R^3 \sin\theta} \psi_\theta + \frac{\cot\theta}{R^2 \sin\theta} \psi_r - \frac{1}{R^2 \sin\theta} \psi_{r\theta}\right)\right] \quad (5e)$$

$$\left(T_r - \frac{R_\theta}{R} T_\theta\right) = 0 \quad (5f)$$

where the capillary number Ca is given by

$$Ca = \frac{\gamma A r_b}{\sigma_0}$$

Equation (5c) is the kinematic boundary condition at the deformable bubble surface, and Eqs. (5d) and (5e) represent shear and normal-stress balances. The volume of the bubble is assumed to remain constant,

$$\int_0^\pi R(\theta)^3 \sin\theta \, d\theta = V \quad (6)$$

where V is the dimensionless volume of the gas bubble.

Because the center of mass of the bubble is fixed at the origin of the coordinate system, the shape of bubble $R(\theta)$ must satisfy a requirement of the following form:

$$\int_0^\pi R^4(\theta) \sin\theta \cos\theta \, d\theta = 0 \quad (7)$$

Since the shape of the bubble is symmetric along $\theta = 0$ and π,

$$R_\theta(0) = R_\theta(\pi) = 0 \quad (8)$$

Solution Procedure

Both the interface shape and terminal velocity of the bubble are unknown a priori and must be determined as part of the overall solution procedure. By assigning a specific bubble shape and terminal velocity and temporarily discarding the normal-stress condition [Eq. (5d)], a complete solution of the velocity and temperature field can be determined from Eqs. (2) and boundary conditions (5). A new bubble shape is computed to satisfy the normal-stress boundary condition. When the prescribed terminal velocity is not correct, the center of the bubble drifts away from the origin of the coordinates, rendering the transformed temperature field unsteady. To ensure the steady character of the transformed temperature field, the terminal velocity is adjusted iteratively to satisfy the condition that the center of mass coincides with the origin.

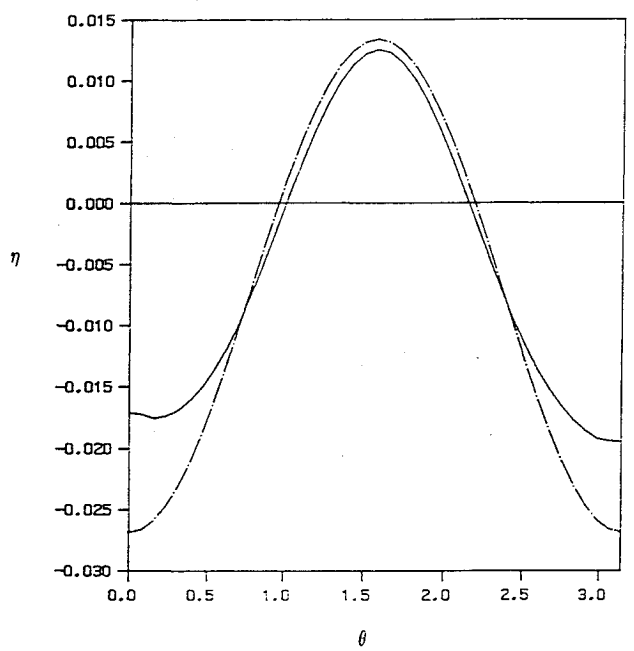

Fig. 2 Surface deflection of the gas bubble vs θ for $Re = 50$, $Ma = 50$, and $Ca = 0.5$ (the broken curve represents the results of the asymptotic method[5] and the solid curve represents the present results).

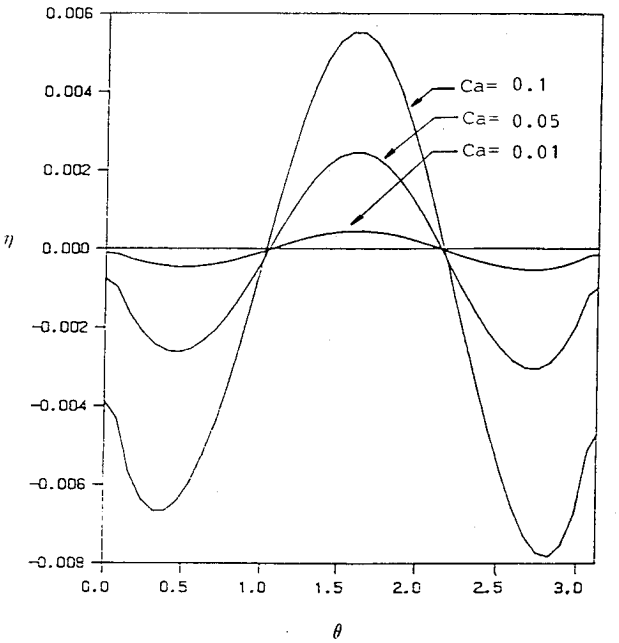

Fig. 3 Surface deflection of the gas bubble vs θ for $Re = 10$, $Ma = 10$, and $Ca = 0.01$, 0.05, and 0.1.

The numerical technique, which is an extended version of that used previously by Lee and Chen[11] to investigate thermocapillary convection around a deformable bubble, has been used to solve system (2) with conditions (5–8). In the code, the irregular physical domain is transformed to a rectangular computational domain by using a boundary-fitted method developed by Thompson et al.,[12] and grid-stretching transformations are used to provide good resolution near the deformed bubble surface. Central-difference formulas with second-order accuracy are used for all spatial derivatives.

When a given estimated shape $R(\theta)$ for the bubble interface is incorrect, the normal stress on the interface is unable to balance the thermocapillary force. The imbalance $\varepsilon(x)$ can be written in the form

$$\varepsilon(\theta) = p - 2\left[\frac{-\psi_{\theta r} + \psi_\theta/R - R_\theta \psi_{rr}}{R^2 \sin\theta}\right] + \frac{R_\theta}{R}\left[\psi_{rr} + \frac{-1}{R^2} \psi_{\theta\theta} - \frac{\cot\theta}{R^2} \psi_\theta\right] + Ca^{-1}\left[\frac{R^2 + 2R_\theta^2 - RR_{\theta\theta}}{(R^2 + R_\theta^2)^{3/2}} + \frac{|R_\theta \cos\theta - R \sin\theta|}{R \sin\theta (R^2 + R_\theta^2)^{1/2}}\right](1 - CaT) \quad (9)$$

The pressure term in Eq. (9) is obtained by integrating the tangential component of the momentum equation along the bubble surface. The imbalance $\varepsilon(\theta)$ may be unequal to zero due to an incorrect interface shape. By forcing $\varepsilon(\theta)$ to be

equal to zero, we get a new bubble shape $R^*(\theta)$, which must satisfy the following equation:

$$p - 2\left[\frac{-\psi_{\theta r} + \psi_\theta/R^* - R_\theta\psi_{rr}}{R^{*2}\sin\theta}\right] + \frac{R_\theta}{R^*}\left[\psi_{rr} + \frac{-1}{R^{*2}}\psi_{\theta\theta} - \frac{\cot\theta}{R^{*2}}\psi_\theta\right] + Ca^{-1}\left[\frac{R^{*2} + 2R_\theta^{*2} - R^*R_{\theta\theta}}{(R^{*2} + R_\theta^{*2})^{3/2}} + \frac{|R_\theta^*\cos\theta - R^*\sin\theta|}{R^*\sin\theta(R^{*2} + R_\theta^{*2})^{1/2}}\right](1 - CaT) = 0 \quad (10)$$

The new bubble shape $R^*(\theta)$ obtained from Eq. (10) must satisfy the constraint of volume conservation:

$$\int_0^\pi R^{*3}(\theta)\sin\theta\,d\theta = V \quad (11)$$

The integral constant included in the pressure and $R^*(\theta)$ can be obtained by Eqs. (10) and (11) using the bisection method.

The requirement that the center of mass of the bubble remain at the origin provides a condition to check whether the guessed terminal velocity is correct. We define

$$M = \int_0^\pi R^4(\theta)\sin\theta\cos\theta\,d\theta \quad (12)$$

Integrations are carried out starting from a guess terminal velocity until M approaches zero.

A brief summary of our computational procedure is as follows.

1) Guess an initial migration velocity. Usually we take the solution for an ideal spherical bubble as the initial migrational velocity.

2) An initial spherical shape of the bubble interface is chosen.

3) The boundary-fitted curvilinear coordinate system that has coordinate lines coincident with the current boundaries is generated numerically.

4) Initial values for ψ, ω, and T over the entire domain are selected.

5) The vorticity equation is solved using initial guesses to form the nonlinear terms in Eq. (2a) and boundary conditions (5a), (5b), and (5e).

6) The stream function and temperature equations are solved iteratively using the successive-line-over-relaxation (SLOR) method. The iteration process is considered converged when the relative error of two successive iterations at a given point is with some specified tolerance, generally taken as 10^{-4}.

7) The new solutions of stream function and temperature are then used to correct the initial guesses of ψ and T.

8) Repeat steps 5–7 iteratively until the relative error of two successive iterations are within a specified value, generally taken as 10^{-4}.

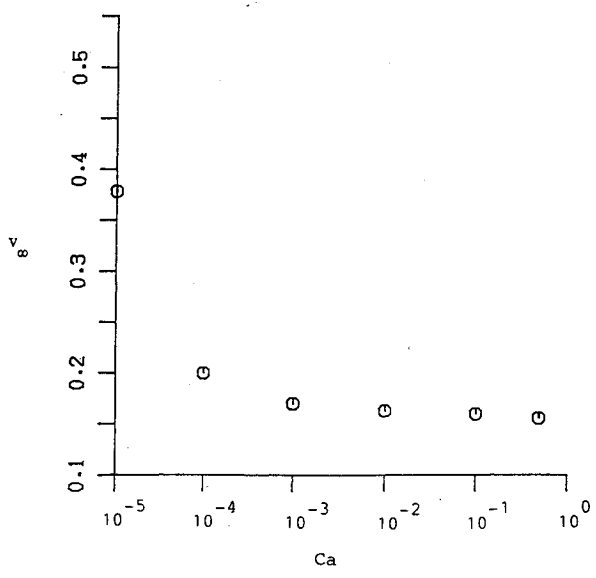

Fig. 4 Terminal-migration velocity v_∞ vs Ca for Re = 10 and Ma = 10.

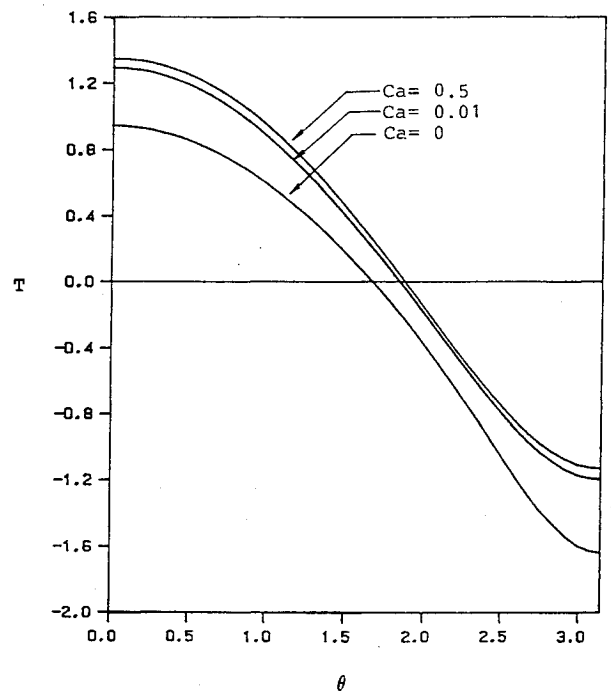

Fig. 5 Temperature distribution on the bubble surface for Re = 10 and Ma = 10 with different Ca.

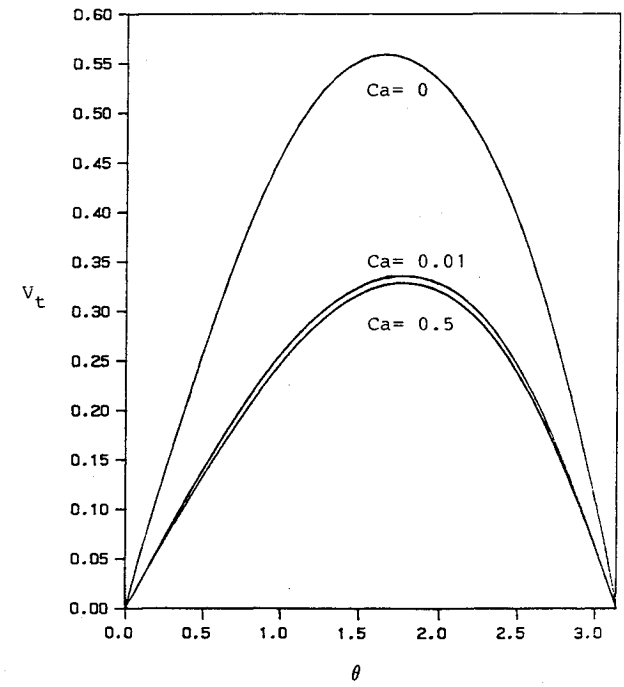

Fig. 6 Tangential velocity distribution on the bubble surface for Re = 10 and Ma = 10 with different Ca.

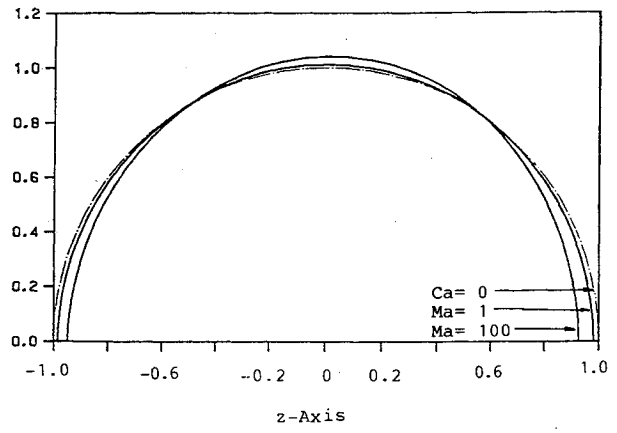

Fig. 7 Surface deformation of the gas bubble for $Pr = 1$ and $Ca = 0.5$ with $Ma = 1$ and 10^2.

9) The new shape of the bubble interface is determined from Eqs. (10) and (11).

10) Return to step 3 and repeat iteratively until $\varepsilon(\theta) < 5 \times 10^{-3}$.

11) Calculate the value M from Eq. (12). If $M < M_c$ (generally taken as $Mc = 10^{-6}$), stop. Otherwise, return to step 1 and repeat until $M < M_c$.

Results and Discussion

The numerical computations described in the preceding section were performed in double-precision arithmetic on the National Central University VAX 8650 computer. The computational domain must be chosen to be large enough to approximate the theoretical assumption of an infinite domain. For computations performed here, the computation domain was selected as $1 \le r \le 5$ and $0 \le \theta \le \pi$. The justification for this selection was demonstrated by Balasubramaniam and Lavery.[5] The problem for a spherical bubble shape ($Ca = 0$) has been studied numerically in Refs. 4 and 5. To check our results, the calculations have been repeated with the same condition chosen by Ref. 5. The present results show good agreement with those of Ref. 5. The number of grid points used in the computational domain influences the accuracy of the results. To determine the proper number of grid points, calculations were performed using different grids. For $Re = 1$, $Ma = 0.1$, and $Ca = 0.01$, the terminal velocities of a bubble for grids of 31×31, 41×41, and 51×51 points are 0.1395, 0.1924, and 0.1919, respectively. For $Re = 10^2$, $Ma = 10^2$, and $Ca = 0.1$, the terminal velocities for 41×41 and 51×51 grid points are 0.1320 and 0.1360, respectively. For $Ma = 10^2$, the difference in the terminal velocities calculated using grids of 41×41 and 51×51 is <3%. For the results that will be discussed later, the grid was selected as 41×41 to save CPU time.

Recently, Balasubramaniam and Chai[6] used an asymptotic method to calculate the bubble shape. From their results, the deviation η of a bubble from a spherical shape can be expressed in following form:

$$\eta(\theta) = R(\theta) - 1 = -(3/32)v_\infty^2 ReCa(3\cos^2\theta - 1) \quad (13)$$

This solution is valid when the surface deformation is small ($\eta \ll 1$). On the contrary, the present method does not have this restriction. In Fig. 2, the surface deflections determined by the present computation and Eq. (13) are compared as a function of θ. Both results show that the shape of the gas bubble deforms to be an oblate ellipsoid with an elongation in the direction perpendicular to the freestream. They are in good agreement for $0.75 < \theta < 2.4$. Below $\theta = 0.75$ or above $\theta = 2.4$, they begin to diverge with the numerical results predicting lower deformations. The solution of Eq. (13) yields a bubble shape that is symmetric fore and aft, i.e., about $\theta = \pi/2$. Because of the inertia effect associated with the thermocapillary migration, the numerical results show a bubble that tilts away from the oncoming flow with the deflection at the front ($\theta = 0$) being smaller than that at the rear ($\theta = \pi$). From Fig. 2, it appears that the surface deflection computed by the present method is more physically realistic. The capillary number, which represents the ratio of maximum differences in surface tension on the gas-liquid interface to mean surface tension σ_0, governs the degree of surface deformation of the bubble. Figure 3 shows the computed deflections of the bubble surface with different Ca for $Re = Ma = 10$. As expected, the results show that the surface deflection is more significant for higher Ca. At the high Ca, the bubble becomes more oblate and oblique.

Of interest is the variation of the terminal-migration velocity of the bubble with Ca. In Fig. 4, the magnitude of the terminal-migration velocity is plotted as a function of Ca for $Re = Ma = 10$. As $Ca \to 0$, the magnitude of terminal velocity approaches that of an ideal spherical bubble ($V_\infty = 0.376$). The terminal velocity decreases exponentially with increasing Ca until $Ca = 10^{-3}$. The variation with Ca is not very significant for $Ca > 10^{-3}$.

Figure 5 displays the temperature distribution along the bubble surface for $Re = 10$ and $Ma = 10$ with different Ca. For the portion of bubble surface $2.5 < \theta < \pi$, the temperature gradients for $Ca > 0$ are smaller than those for $Ca = 0$. The reduction of temperature gradient results in a decrease of shear stress at the interface. This is the major reason for the reduction in terminal-migration velocity observed for bubbles with deformed surfaces. Figure 6 shows the tangential velocity distribution along the bubble surface for $Re = 10$ and $Ma = 10$ with different Ca. When $Ca = 0$, the tangential velocity V_t is exactly the θ component of velocity v. It is clear that the tangential velocity along the bubble surface decreases with increasing Ca as a result of the reduction in shear stress.

The influence of Ma on the surface deformation of the bubble is shown in Fig. 7 for $Pr = 1$ and $Ca = 0.5$. The

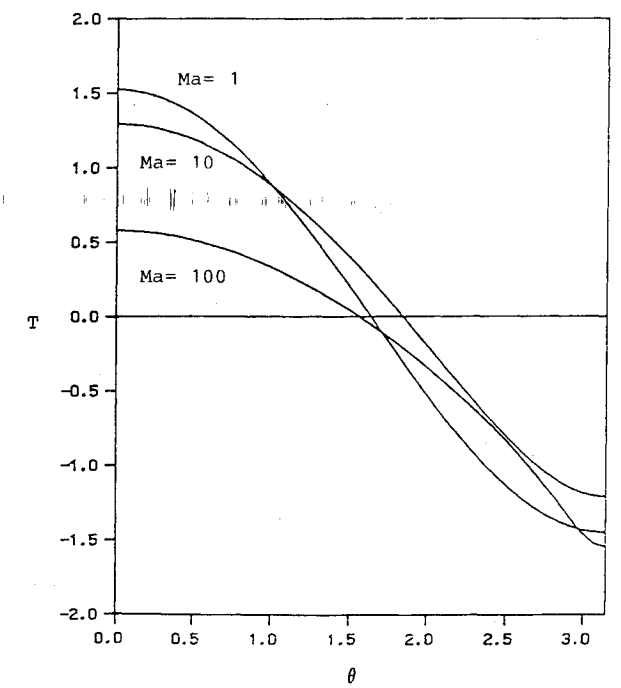

Fig. 8 Temperature distribution on the bubble surface for $Ca = 0.5$ and $Pr = 1$ with different Ma.

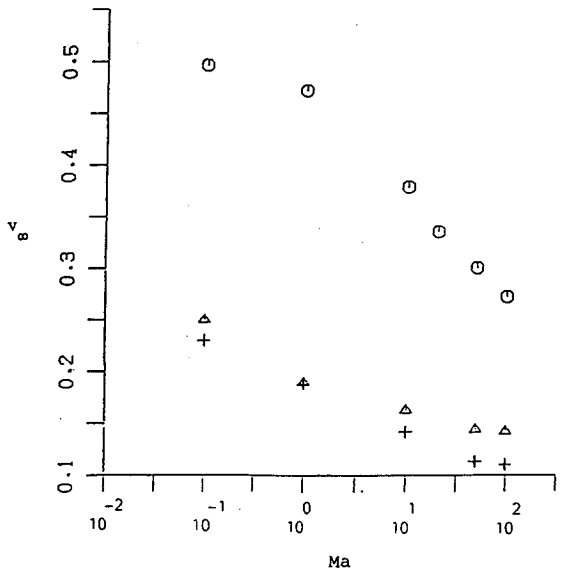

Fig. 9 Terminal-migration velocity v_∞ vs *Ma* for *Pr* = 1: ○ *Ca* = 0; △ *Ca* = 0.01; + *Ca* = 0.5.

results show that with increasing *Ma* the gas bubble tends to elongate in the cross-stream direction and deforms more oblately. Figure 8 displays the temperature distribution along the bubble surface for $Ca = 0.1$ and $Pr = 1$ with $Ma = 1$, 10, and 10^2. It is obvious that the temperature gradient along the bubble surface is reduced by increasing the strength of convective effects (larger *Ma*). The effect of *Ma* on the terminal-migration velocity of the bubble for different *Ca* is shown in Fig. 9. The present results of $Ca > 0$ are similar to those of $Ca = 0$ in that the terminal velocity decreases with increasing *Ma*. The terminal velocity for $Ca > 0$ is smaller than that for $Ca = 0$, and it tends to an asymptotic value for large *Ma*. The difference in terminal velocity between an ideal spherical bubble and a deformable bubble becomes less significant when *Ma* increases.

Conclusions

Numerical computations have been performed to study the thermocapillary migration of a deformable gas bubble placed in a liquid with a constant temperature gradient. The surface deformation of the bubble is sensitive to the value of capillary and Marangoni numbers. The shape of the bubble deforms to an oblate ellipsoid with elongation in the direction normal to the moving direction and tilting backward slightly. The scaled terminal-migration velocity is reduced significantly when the deformation effect of the bubble is taken into account, so that the terminal-migration velocity will be overestimated if the bubble shape is assumed to be spherical.

Acknowledgment

This work was supported by the National Science Council of the Republic of China.

References

[1]Young, N. O., Goldstein, J. S., and Block, M. J., "The Motion of Bubbles in a Vertical Temperature Gradient," *Journal of Fluid Mechanics*, Vol. 6, Oct. 1959, pp. 350–356.

[2]Bratukhin, Y. K., "Thermocapillary Drift of a Viscous Fluid Droplet," *Fluid Dynamics*, Vol. 10, 1975, pp. 833–837.

[3]Subramanian, R. S., "Slow Migration of a Gas Bubble in a Thermal Gradient," *American Institute of Chemical Engineering Journal*, Vol. 27, No. 4, July 1981, pp. 646–654.

[4]Shankar, N., and Subramanian, R. S., "The Stokes Motion of a Gas Bubble Due to Interface Tension Gradients at Low to Moderate Marangoni Numbers," *Journal of Colloid Interface Sciences*, Vol. 123, No. 2, June 1988, pp. 512–523.

[5]Balasubramaniam, R., and Lavery, J. E., "Numerical Simulation of Thermocapillary Bubble Migration Under Microgravity for Large Reynolds and Marangoni Numbers," *Numerical Heat Transfer A*, Vol. 16, No. 2, Sept. 1989, pp. 175–187.

[6]Balasubramaniam, R., and Chai, A. T., "Thermocapillary Migration of Droplet: An Exact Solution for Small Marangoni Numbers," *Journal of Colloid Interface Sciences*, Vol. 119, No. 2, Oct. 1987, pp. 531–538.

[7]Ryskin, G., and Leal, L. G., "Numerical Solutions of Free-Boundary Problems in Fluid Mechanics," *Journal of Fluid Mechanics*, Vol. 148, Nov. 1984, pp. 1–17.

[8]Christov, C. I., and Volkov, P. K., "Numerical Investigation of the Steady Viscous Flow Past a Stationary Deformable Bubble," *Journal of Fluid Mechanics*, Vol. 158, Sept. 1985, pp. 341–364.

[9]Chen, J. C., Sheu, J. C., and Jwu, S. S., "Numerical Computation of Thermocapillary Convection in a Rectangular Cavity," *Numerical Heat Transfer A*, Vol. 17, No. 3, April 1990, pp. 287–308.

[10]Chen, J. C., Sheu, J. C., and Lee, Y. T., "Maximum Stable Length of Nonisothermal Liquid Bridges," *Physics of Fluids A*, Vol. 2, No. 7, July 1990, pp. 1118–1123.

[11]Lee, Y. T., and Chen, J. C., "Numerical Investigation of Thermocapillary Flow Around a Deformable Bubble on the Hot Wall," *Journal of the Chinese Society of Mechanical Engineers*, Vol. 11, No. 3, June 1990, pp. 233–243.

[12]Thompson, J. F., Thames, F. C., and Mastin, W., "Automatic Numerical Generation of Body Fitted Curvilinear Coordinate System for Field Containing Any Number of Arbitrary Two-Dimensional Bodies," *Journal of Computational Physics*, Vol. 15, No. 3, July 1974, pp. 299–319.

[13]Middlecoff, J. F., and Thamas, P. D., "Direct Control of the Grid Point Distribution in Meshes Generated by Elliptic Equations," *AIAA Journal*, Vol. 18, No. 6, 1980, pp. 652–656.